Liquidus Phase Relations and Solid-Liquid Partitioning in the Fe-Si-C System Under Core Pressures

Masahiro Hasegawa[1], Kei Hirose[1,2], Kenta Oka[1], and Yasuo Ohishi[3]

[1]Department of Earth and Planetary Science, The University of Tokyo, Tokyo, Japan
[2]Earth-Life Science Institute, Tokyo Institute of Technology, Tokyo, Japan
[3]Japan Synchrotron Radiation Research Institute, SPring-8, Hyogo, Japan

Abstract Both silicon and carbon have been proposed to be important light elements in the Earth's core, in particular in the inner core. Here we performed melting experiments on the Fe-Si-C ternary system at ~50, ~136, and ~200 GPa and determined the liquidus phase relations and the solid/liquid partition coefficients (D) of C and Si. The liquidus field of Fe shrinks at higher pressures, which narrows down the possible outer core liquid composition. Our data also demonstrate that the Fe-Si binary eutectic liquid reduces its Si concentration to ~8 wt% with increasing pressure to 330 GPa. We found that the inner core is not Fe-Si-C-S alloy but likely includes hydrogen when considering the low D_C and the strong enhancement of D_{Si} with increasing liquid C abundance. The present-day core does not include as much as ~6 wt% Si, suggesting that at least a part of "missing" Si could be sequestrated elsewhere.

Plain Language Summary Chemical compositions of both the liquid outer core and solid inner core are not known yet. Recent theoretical calculations argued that the inner core density and velocities are best explained with an Fe-Si-C alloy. Here we performed melting experiments in the Fe-Si-C system to middle outer core pressures, based on in-situ phase identification and ex-situ textural and compositional characterizations using electron microprobes. The results demonstrate 1) a compositional range of liquid that first crystallizes Fe in the Fe-Si-C ternary system and 2) the solid/liquid partition coefficients, D_C and D_{Si}, between solid and liquid Fe. The compositions of Fe-Si-C-S liquids in equilibrium with the previously proposed inner core solids are calculated using these D_C, D_{Si}, and previously known D_S. We found, however, that such Fe-Si-C-S liquids cannot represent the outer core because they do not crystallize Fe at inner core conditions. It suggests that the inner core includes hydrogen as a major light element. In addition, the

high Mg/Si ratio in the Earth's upper mantle compared to those of chondrites implies ~6 wt% Si in the core, but the present results indicate at least a part of such "missing" Si is present elsewhere.

1. Introduction

Both the Earth's outer and inner core are less dense than liquid and solid pure Fe by ~8% and ~4%, respectively (Kuwayama et al., 2020; Vočadlo et al., 2003; Fei et al., 2016). It indicates the presence of certain amounts of light elements, but they have not been identified yet. Both silicon and carbon have been proposed to be major light elements in the core (Hirose et al., 2013; Li and Fei, 2014). This is supported by the recent ab initio calculations performed by Li et al. (2018), demonstrating that solid Fe-Si-C alloy best explains the density, shear and compressional velocities observed in the inner core.

Melting phase relations in Fe alloy systems help constrain the possible liquid core composition. Those in the Fe-Si (Kuwayama & Hirose, 2004; Fischer et al., 2012, 2013; Ozawa et al., 2016) and Fe-C binary systems (Fei & Brosh, 2014; Mashino et al., 2019) have been examined to core pressures. Recently Miozzi et al. (2020) carried out high-pressure experiments on $Fe_{93}Si_3C_4$ alloy and argued the likelihood of Fe-Si-C core. Previous experimental studies on ternary Fe alloy systems revealed strong interactions between light impurity elements which can lead to liquid-liquid immiscibility and limited simultaneous solubility in molten Fe. Earlier experiments below 4 GPa showed that the solubility of C into liquid Fe is diminished in the presence of Si (Takahashi et al., 2013; Li et al., 2015). Such strong non-ideal interaction between Si and C might be involved in the liquidus phase relations, even under the core pressure range.

Here we performed melting experiments up to 199 GPa and examined the liquidus phase relations, in particular the liquidus field of Fe (a compositional range of liquid that first crystallizes Fe) under core pressures based on in-situ phase identification and ex-situ textural and compositional characterizations. We also determined the solid/liquid partition coefficients D_C and D_{Si} in the Fe-Si-C ternary system and found that the latter is remarkably enhanced with increasing C concentration in liquid. The possible outer and inner core compositions are discussed on the basis of these new experimental data.

2. Experimental Results

We conducted thirteen separate melting experiments at the pressures of ~50 GPa, ~136 GPa, and ~200 GPa (see Experimental Methods in the supporting information) (Table S1). In addition, we determined C concentrations in liquids formed in runs #HOFeSi08 and #KH reported in Ozawa et al. (2016).

2.1. Melting Textures

In each sample cross-section, there was a chemically homogeneous area with a non-stoichiometric composition at the center of a laser-heated spot, which should represent a quenched liquid alloy (Figure 1). The incorporation of Al_2O_3 grains into a metal part and eventually the formation of mashroom-shaped metal are the strong evidence to back up that the laser-heated spot was melted.

In contact with a quenched liquid pool, we found the layers of single-phase Fe, Fe-Si, Fe_3C, or combination of those (Figure 1). Such single-phase solid layer represents the liquidus phase for (the solid phase first crystallizing from) a liquid formed in each experiment. Solid Fe containing minor amounts of Si was observed in runs #1, 3, 4, 5, and 6, indicating that the compositions of coexisting liquids are within the liquidus field of Fe. XRD analyses at 48 GPa confirmed its crystal structure to be fcc (Fig. S1 in the supporting information). On the other hand, Si-rich solid Fe-Si alloys were found in runs #2, 7–9, 12, and 13, constraining the liquidus field of Fe-Si. They exhibited CsCl-type B2 structure that has been typically observed for Si-rich Fe alloys (e.g., Kuwayama et al., 2009; Fischer et al., 2013). We obtained two solid-phase layers, Fe + Fe_3C and Fe + Fe-Si, in runs #10 and #11, respectively, implying that quenched liquids in these runs represent cotectic liquids in the Fe-Si-C ternary system. A subsolidus part was found outside of the liquidus phase layer where temperature was relatively low because of a temperature gradient in a laser-heated sample (Figure 1a).

2.2. Liquidus Phase Relations in Fe-Si-C

These results constrain the liquidus phase relations in the Fe-Si-C ternary system at approximately 50 GPa, 136 GPa, and 200 GPa (Figures 2a–c). The cotectic lines (the intersection of liquidus surfaces on which liquids coexist with two solid phases) are drawn based not only on liquid compositions coexisting with one or two liquidus phases but also on their systematic shifts with increasing pressure (Figure 2d). The binary eutectic liquid composition and eutectic temperature in the Fe-C system have been experimentally studied

96 up to 255 GPa (Mashino et al., 2019) and are helpful for obtaining the ternary liquidus
97 phase diagrams.

98 At ~50 GPa, the position of the Fe + Fe-Si cotectic line (the boundary between the liquidus
99 fields of Fe and Fe-Si) is relatively well constrained from the compositions of liquids
100 coexisting with Fe and Fe-Si, respectively (Figure 2a). The Fe + Fe_3C cotectic line is
101 obtained from the compositions of liquids coexisting with Fe, including a previous datum
102 reported by Miozzi et al. (2020), and the Fe-Fe_3C binary eutectic liquid composition
103 (Mashino et al., 2019). Solid Fe and Fe-Si found as liquidus phases contained 10.3(2) wt%
104 Si (maximum) and 14.6(2) wt% Si, respectively, indicating that the Fe-Si binary eutectic
105 point is located between these two Si abundances (Figure 3). The geometrical constraint on
106 the ternary liquidus phase diagram suggests that the Fe-FeSi binary eutectic point is located
107 around 11.5 wt% of Si, which is in agreement with the results by Fischer et al. (2012,
108 2013).

109 At ~136 GPa, the liquidus field of Fe is constrained by the compositions of three Fe-Si-C
110 liquids coexisting with solid Fe (Figure 2b). The position of the ternary eutectic point
111 should move toward carbon-rich side as pressure increases (Figure 2d) because the dT/dP
112 slope is greater for the Fe-Si melting curve than that for Fe-C (Morard et al., 2017). The
113 Fe-C binary eutectic liquid composition changes very little with increasing pressure above
114 50 GPa and includes ~4 wt% C at this pressure range (Mashino et al., 2019). The liquid Fe
115 containing 10.8(2) wt% Si and 0.1(1) wt% C coexisted with solid Fe-Si, indicating the
116 upper bound for Si concentration in the Fe-FeSi binary eutectic liquid. The lower bound is
117 given by the maximum Si content (6.7(1) wt%) in solid Fe obtained at this pressure range.
118 Furthermore, the geometrical constraint on cotectic lines suggests ~10 wt% of Si in the
119 Fe-FeSi binary eutectic liquid (Figure 3).

120 At ~200 GPa, we obtained liquids coexisting with Fe + Fe_3C in run #10 and Fe + Fe-Si in
121 run #11. They place tight constraints on the locations of the Fe + Fe_3C and Fe + Fe-Si
122 cotectic lines along with the Fe-C binary eutectic point with ~4 wt% C (Mashino et al.,
123 2019) (Figure 2c). The lower and upper bounds for Si concentration in the Fe-FeSi eutectic
124 liquid are indicated by the maximum 7.9(5) wt% Si in solid Fe and the minimum 15.1(1)
125 wt% Si in solid Fe-Si, respectively (Figure 3). The location of the Fe + Fe-Si cotectic line
126 in the Fe-Si-C ternary diagram suggests ~8.8 wt% Si in the Fe-FeSi binary eutectic liquid.

These results obtained in a pressure range from ~50 to ~200 GPa are extrapolated to the ICB pressure of 330 GPa, indicating that the liquidus field of Fe becomes smaller with increasing pressure (Figure 2d). As mentioned above, higher dP/dT slope of the Fe-Si melting curve than that for Fe-C (Morard et al., 2017) suggests that the Fe-Si-C ternary eutectic point moves toward a composition with higher C/Si ratio as pressure increases. The present experimental results also indicate that the Fe-FeSi binary eutectic point shifts toward the Si-poor side with increasing pressure (see Figure 3 for details); Si concentration decreases from ~11.5 wt% at 50 GPa to ~8.8 wt% at 200 GPa. It is a modest change compared to that reported by Ozawa et al. (2016). The difference is attributed to the fact that Ozawa and others did not consider the presence of carbon in their experiments. The Fe-Si binary eutectic liquid will contain ~8 wt% Si at 330 GPa.

2.3. Solid-Liquid Partitioning of C and Si

The present experiments also show the solid/liquid partition coefficients of C and Si, D_C and D_{Si}, between coexisting solid Fe and liquid Fe-Si-C. We also obtained D_C in the Si-free Fe-C system (Mashino et al., 2019) and D_{Si} in the C-free Fe-Si system (Kuwayama & Hirose, 2004). These D_C and D_{Si} are plotted as a function of the liquid abundances of Si and C, respectively. The D_C values range from <0.1 to 0.2(1), and the effect of Si is not clear (Figure 4a). On the other hand, D_{Si} is positively correlated with C concentration in liquid; it markedly increases from D_{Si} = 1.0 at 0 wt% C to D_{Si} = 2.8 at 5 wt% C (Figure 4b). Indeed, such positive correlation is known at atmospheric pressure (Hino and Ito, 2010). Compared to the 1-bar data on bcc Fe, the present experiments demonstrate a larger effect of C on D_{Si} between fcc/hcp Fe and liquid. The pressure dependence of D_{Si} is not clearly observed in the present data collected in a pressure range from 34 to 199 GPa.

3. Discussion

3.1. Constraints on Outer Core Composition

The density jump across the ICB is greater than the density difference between solid and liquid iron at 330 GPa, indicating that the solid inner core is depleted in light elements compared to the liquid outer core. It requires the liquid outer core composition to be within the liquidus field of Fe at 330 GPa such that solid Fe crystallizes at the ICB (Figure 2d). The liquidus field of Fe corresponds to a compositional range on the Fe-rich side of the eutectic rather than light-element-rich sides. The Fe-Si and Fe-C eutectic liquids include ~8

wt% Si (Figure 3) and <4 wt% C (Mashino et al., 2019), respectively, at ICB conditions, which tells the upper bounds for Si and C concentrations in the outer core that crystallizes the denser inner core. The present results on the Fe-Si-C ternary liquidus phase relations narrow down the possible compositional range of the liquid outer core when Si and C are major light elements (Figure 2d).

The recent ab initio calculations by Li et al. (2018) argued that hcp $Fe_{30}Si_1C_1$ (Fe-1.6wt%Si-0.7wt%C) alloy best explains the density, compressional and shear velocities of the inner core when its temperature is 6500 K at 360 GPa. If it represents the inner core composition, the composition of the liquid outer core is calculated to be Fe containing 0.4–0.7 wt% Si and 3.5–7 wt% C based on D_C = 0.1–0.2 and D_{Si} = 2.3–3.5 (Figure 4). The Fe-Si-C ternary liquidus phase relations at 330 GPa shown in Figure 2d indicates that such range of liquid composition is only marginally within the liquidus field of Fe at Fe + 0.4–0.7 wt% Si + 3.5–3.9 wt% C. Furthermore, the outer core liquid may include some oxygen, which is not distributed into the solid inner core (Alfè et al., 2002; Ozawa et al., 2010; Yokoo et al., 2019). The liquid Fe + 0.4–0.7 wt% Si + 3.5–3.9 wt% C + 1–2 wt% O can account for the observed outer core density and velocity according to the ab initio calculations performed by Badro et al. (2014) with T_{ICB} = 6300 K and more recently by Umemoto & Hirose (2020) with T_{ICB} = 6000 K.

Li et al. (2018) also proposed the possible range of the inner core composition in the Fe-Si-C-S system. Sulfur concentration in the core has been relatively well constrained to be 1.7 wt% from its chondritic and mantle abundances (Dreibus & Palme, 1996). Previous calculations and experiments have shown the solid/liquid partition coefficient of sulfur D_S = 0.8 at ICB conditions (Alfè et al., 2002; Yokoo et al., 2019), suggesting that the inner core may include 1.4 wt% (2.3 atm%) S. The calculations by Li et al. (2018) gave the possible Si and C contents jointly with 1.4 wt% S in the inner core at 360 GPa and 5500/6000/6500 K. Subsequently we calculated the corresponding Si and C concentrations in liquid Fe-Si-C-1.7wt%S alloys that are in equilibrium with such inner core solid compositions at ICB conditions using the D_C (=0.1, 0.2) and D_{Si} values shown above, as illustrated in Figures 2e and 2f. Most of these Fe-Si-C liquid compositions are in the liquidus field of Fe_7C_3 and thus cannot represent the outer core (Li et al., 2016) (note that the addition of 1.7 wt% S to the Fe-Si-C system does not expand the liquidus field of Fe).

Only the Fe-Si-C liquid compositions calculated with D_C = 0.2 and T_{360GPa} = 6500 K are within the liquidus field of Fe.

However, the 6500 K at 360 GPa corresponds to >6280 K at the ICB and >4620 K at the core-mantle boundary (CMB) when Grüneisen parameter γ = 1.5 is applied for the entire core (Vočadlo et al., 2003). The solidus temperature of the mantle has been determined to be ~4150 ± 150 K by Fiquet et al. (2010) and Andrault et al. (2011) or ~3500 ± 200 K more recently by Nomura et al. (2014) and Kim et al. (2020). T_{CMB} > 4620 K is much higher than any of these estimates and therefore T_{ICB} > 6280 K is unlikely, otherwise the lowermost mantle should be molten not only locally at ultra-low velocity zones but globally. These suggest that the inner core is not an Fe-Si-C-S alloy but likely includes hydrogen as a major light element (note that oxygen is not soluble into solid Fe in the inner core as mentioned above).

3.2. Missing Si in the Core?

The Mg/Si molar ratio in the upper mantle (~1.3) is known to be markedly higher than those of chondrites (~0.7–1.0) and the solar system (1.0), which is referred to "missing Si problem". Such high Mg/Si ratio may be reconciled with a perovskititic lower mantle (Murakami et al., 2012; Mashino et al., 2020). Or, it has been repeatedly suggested that it is attributed to the presence of 5–7 wt% Si in the core (O'Neill, 1991; Allègre et al., 1995). The incorporation of ~6 wt% Si into the core could also cause the difference in the $^{30}Si/^{28}Si$ isotopic ratio observed between terrestrial rocks and meteorites (e.g., Georg et al., 2007; Shahar et al., 2009).

The presence of 6 wt% Si in liquid Fe allows crystallization of solid Fe at the ICB if the system is Fe-Si binary since its eutectic liquid includes ~8 wt% Si at 330 GPa (Figure 3). However, the density and velocity observed in the outer core cannot be explained by the 6 wt% Si alone. While the earlier calculations by Badro et al. (2014) suggested only <5 wt% Si in the liquid core, the more recent ones by Umemoto & Hirose (2020) permit 6 wt% Si + 1.7 wt% S in company with either 2.3 wt% O, 1.7 wt% C, or 0.25 wt% H in the outer core when T_{ICB} = 5400 K and Fe/Ni =16 by weight. It gives Fe-1.4wt%S-6wt%Si, Fe-1.4wt%S-9.8wt%Si-0.2–0.3wt%C, or Fe-1.4wt%S-6wt%Si-0.18wt%H for the solid inner core with D_O = 0 (Alfè et al., 2002; Yokoo et al., 2019) and D_H = 0.7 observed at 20 GPa (Imai, 2013) in addition to D_C, D_{Si}, and D_S = 0.8 above. The former two Fe-S-Si(-C)

compositions do not explain the inner core density and velocity according to Li et al. (2018). The calculations by Li and others also show that the density of solid Fe-1.4wt%S-4.8wt%Si ($Fe_{89}S_2Si_9$) at inner core conditions is already similar to the inner core density, indicating that the addition of 0.18 wt% H makes the alloy density much lower than observed. The inner core density may be explained by 0.3 wt% or 0.12(5) wt% H in Fe alone as recently estimated by calculations (Caracas, 2015) and neutron diffraction measurements of Fe-H alloys (Ikuta et al., 2019), respectively.

These suggest that Si concentration in the present-day outer core is less than 6 wt%. Alternatively, it is possible that the Earth's core initially included ~6 wt% Si but reduced its abundance due to Si+O saturation and resulting SiO_2 crystallization upon secular cooling (Hirose et al., 2017; Helffrich et al., 2020). It is also possible that the lower mantle includes $MgSiO_3$ bridgmanite-enriched ancient mantle structures (BEAMS) as suggested by Ballmer et al. (2017) and thus has a lower Mg/Si ratio than the upper mantle.

4. Conclusions

The liquidus phase relations in the ternary Fe-Si-C system were examined to 199 GPa based on a combination of laser-heated DAC, in-situ XRD measurement, and ex-situ textural and chemical analyses. These data demonstrate that the liquidus field of Fe in Fe-Si-C becomes smaller at higher pressures. Extrapolation of the present results to inner core conditions constrains the possible range of the outer core liquid composition when silicon and carbon are major light elements. We also obtained the solid/liquid partition coefficients D_C and D_{Si} and found that D_{Si} is remarkably enhanced with increasing the C content in liquid Fe, while the effect of Si on D_C was not clearly found.

With these solid/liquid partition coefficients, we calculated liquid alloy compositions that are in equilibrium with the possible Fe-Si-C-S solid inner core compositions proposed by recent ab initio calculations (Li et al., 2018). They are marginally within the liquidus field of Fe at 330 GPa only when T_{360GPa} = 6500 K, corresponding to T_{CMB} > 4620 K much higher than the solidus temperature of the lowermost mantle. It suggests that the inner core is not Fe-Si-C-S alloy but includes hydrogen as a major light element. The solid/liquid partitioning of Si obtained in this study also indicates that the present-day core does not include as much as ~6 wt% Si required to compensate the high Mg/Si ratio of the Earth's

mantle compared to those of chondrites and the solar system. The “missing Si problem” may therefore be reconciled with the sequestration of Si elsewhere than in the core.

Data Availability Statement

Datasets for this research are found in Table S1 and Fig. S1 available online (from https://zenodo.org/record/4729062).

Acknowledgments

K. Yonemitsu and Y. Kuwayama are acknowledged for their help in EPMA measurements and data analyses. We thank anonymous reviewers for their valuable comments. XRD measurements were performed at BL10XU, SPring-8 (proposals no. 2019B0072 and 2020A0072). This work was supported by the JSPS grant to K.H.

References

Akahama, Y., & Kawamura, H. (2004). High-pressure Raman spectroscopy of diamond anvils to 250 GPa: method for pressure determination in the multimegabar pressure range. *Journal of Applied Physics*, *96*, 3748–3751.

Alfè, D., Gillan, M. J., & Price, G. D. (2002). Composition and temperature of the Earth's core constrained by combining ab initio calculations and seismic data. *Earth and Planetary Science Letters*, *195*, 91–98.

Allègre, C. J., Poirier J.-P., Humler, E., & Hofmann, A. W. (1995). The chemical composition of the Earth. *Earth and Planetary Science Letters*, *134*, 515–526.

Andrault, D., Bolfan-Casanova, N., Lo Nigro, G., Bouhifd, M. A., Garbarino, G., & Mezouar, M. (2011). Solidus and liquidus profiles of chondritic mantle: implication for melting of the Earth across its history, *Earth and Planetary Science Letters*, *304*, 251–259.

Badro, J., Cote, A. S., & Brodholt, J. P. (2014). A seismologically consistent compositional model of Earth's core. *Proceedings of the National Academy of Sciences of the United States of America*, *111*, 7542–7545.

Ballmer, M., Houser, H., Hernlund, J. W., Wentzcovitch, R. M., & Hirose, K. (2017). Persistence of strong silica-enriched domains in the Earth’s lower mantle. *Nature Geoscience*, *10*, 236–240.

Caracas, R. (2015). The influence of hydrogen on the seismic properties of solid iron. *Geophysical Research Letters*, *42*, 3780–3785.

Dreibus, G., & Palme, H. (1996) Cosmochemical constraints on the sulfur content in the Earth's core. *Geochimica et Cosmochimica Acta*, *60*, 1125–1130.

Fei, Y., & Brosh, E. (2014). Experimental study and thermodynamic calculations of phase relations in the Fe–C system at high pressure. *Earth and Planetary Science Letters*, *408*, 155–162.

Fei, Y., Murphy, C., Shibazaki, Y., Shahar, A., & Huang, H. (2016). Thermal equation of state of hcp-iron: constraint on the density deficit of Earth's solid inner core. *Geophysical Research Letters*, *43*, 6837–6843.

Fiquet, G., Auzende, A. L., Siebert, J., Corgne, A., Bureau, H., Ozawa, H., & Garbarino, G. (2010). Melting of peridotite to 140 gigapascals. *Science*, *329*, 1516–1518.

Fischer, R. A., Campbell, A. J., Caracas, R., Reaman, D. M., Dera, P., & Prakapenka, V. B. (2012). Equation of state and phase diagram of Fe-16Si alloy as a candidate component of Earth's core. *Earth and Planetary Science Letters*, *357-358*, 268–276.

Fischer, R. A., Campbell, A. J., Reaman, D. M., Miller, N. A., Heinz, D. L., Dera, P., & Prakapenka, V. B. (2013). Phase relations in the Fe–FeSi system at high pressures and temperatures. *Earth and Planetary Science Letters*, *373*, 54–64.

Georg, R. B., Halliday, A. N., Schauble, E. A., & Reynolds, B. C. (2007). Silicon in the Earth's core. *Nature*, *447*, 1102–1106.

Helffrich, G. (2014). Outer core compositional layering and constraints on core liquid transport properties. *Earth and Planetary Science Letters*, *391*, 256–262.

Helffrich, G., Hirose, K., & Nomura, R. (2020). Thermodynamical modeling of liquid Fe-Si-Mg-O: molten magnesium silicate release from the core. *Geophysical Research Letters*, *47*, e2020GL089218.

Hino, M., & Ito, K. (2010). Thermodynamic data for steelmaking. Sendai: Tohoku University Press.

Hirao, N., Kawaguchi, S. I., Hirose, K., Shimizu, K., Ohtani, E., & Ohishi, Y. (2020). New developments in high-pressure X-ray diffraction beamline for diamond anvil cell at SPring-8. *Matter and Radiation at Extremes*, *5*, 018403.

Hirose, K., Labrosse, S., & Hernlund, J. (2013). Composition and state of the core. *Annual Review of Earth and Planetary Sciences*, *41*, 657–691.

316 Hirose, K., Morard, G., Sinmyo, R., Umemoto, K., Hernlund, J., Helffrich, G., & Labrosse,
317 S. (2017). Crystallization of silicon dioxide and compositional evolution of the Earth's
318 core. *Nature*, *543*, 99–102.
319 Ikuta, D., Ohtani, E., Sano-Furukwa, A., Shibazaki, Y., Terasaki, H., Yuan, L., & Hattori, T.
320 (2019). Interstitial hydrogen atoms in face-centered cubic iron in the Earth's core.
321 *Scientific Reports*, *9*, 7108.
322 Imai, T. (2013). Crystal/melt partitioning under deep mantle conditions and melting phase
323 relation in the system Fe-FeH. *PhD Thesis, Tokyo Institute of Technology*.
324 Kim, T., Ko, B., Greenberg, E., Prakapenka, V., Shim, S.-H., & Lee, Y. (2020). Low
325 melting temperature of anhydrous mantle materials at the core-mantle boundary.
326 *Geophysical Research Letters*, *47*, e2020GL089345.
327 Kuwayama, Y., & Hirose, K. (2004). Phase relations in the system Fe–FeSi at 21 GPa.
328 *American Mineralogist*, *89*, 273–276.
329 Kuwayama, Y., Sawai, T., Hirose, K., Sata, N., & Ohishi, Y. (2009). Phase relations of
330 iron-silicon alloys at high pressure and high temperature. *Physics and Chemistry of*
331 *Minerals*, *36*, 511–518.
332 Kuwayama, Y., Morard, G., Nakajima, Y., Hirose, K., Baron, A. Q. R., Kawaguchi, S. I. et
333 al. (2020). Equation of state of liquid iron under extreme conditions. *Physical Review*
334 *Letters*, *124*, 165701.
335 Li, J., & Fei, Y. (2014). Experimental constraints on core composition. *Treatise on*
336 *Geochemistry*, (2nd ed., Vol. 3, pp. 527–557). Amsterdam: Elsevier.
337 Li, Y., Dasgupta, R., & Tsuno, K. (2015). The effects of sulfur, silicon, water, and oxygen
338 fugacity on carbon solubility and partitioning in Fe-rich alloy and silicate melt systems
339 at 3 GPa and 1600°C: implications for core–mantle differentiation and degassing of
340 magma oceans and reduced planetary mantles. *Earth and Planetary Science Letters*,
341 *415*, 54–66.
342 Li, Y., Vočadlo, L., Brodholt, J., & Wood, I. G. (2016). Thermoelasticity of Fe_7C_3 under
343 inner core conditions. *Journal of Geophysical Research: Solid Earth*, *121*, 5828–5837.
344 Li, Y., Vočadlo, L., & Brodholt, J. P. (2018). The elastic properties of hcp-Fe alloys under
345 the conditions of the Earth's inner core. *Earth and Planetary Science Letters*, *493*, 118–
346 127.

Mashino, I., Miozzi, F., Hirose, K., Morard, G., & Sinmyo, R. (2019). Melting experiments on the Fe–C binary system up to 255 GPa: constraints on the carbon content in the Earth's core. *Earth and Planetary Science Letters*, *515*, 135–144.

Mashino, I., Murakami, M., Miyajima, N., & Petitgirard, S. (2020). Experimental evidence for silica–enriched Earth's lower mantle with ferrous iron dominant bridgmanite. *Proceedings of the National Academy of Sciences of the United States of America*, *117*, 27899–27905.

Miozzi, F., Morard, G., Antonangeli, D., Baron, M. A., Boccato, S., Pakhomova, A. et al. (2020). Eutectic melting of Fe-3 at% Si-4 at% C up to 200 GPa and implications for the Earth's core. *Earth and Planetary Science Letters*, *544*, 116382.

Morard, G., Andrault, D., Antonangeli, D., Nakajima, Y., Auzende, A. L., Boulard, E., et al. (2017). Fe–FeO and Fe–Fe_3C melting relations at Earth's core–mantle boundary conditions: implications for a volatile–rich or oxygen–rich core. *Earth and Planetary Science Letters*, *473*, 94–103.

Mori, Y., Ozawa, H., Hirose, K., Sinmyo, R., Tateno, S., Morard, G., & Ohishi, Y. (2017). Melting experiments on Fe–Fe_3S system to 254 GPa. *Earth and Planetary Science Letters*, *464*, 135–141.

Murakami, M., Ohishi, Y., Hirao, N., & Hirose, K. (2012). A perovskitic lower mantle inferred from high-pressure, high-temperature sound velocity data. *Nature*, *485*, 90–95.

Nomura, R., Hirose, K., Uesugi, K., Ohishi, Y., Tsuchiyama, A., Miyake, A., & Ueno, Y. (2014). Low core-mantle boundary temperature inferred from the solidus of pyrolite. *Science*, *343*, 522–525.

O'Neill, H. C. (1991). The origin of the Moon and the early history of the Earth: a chemical model: 2. The Earth. *Geochimica et Cosmochimica Acta*, *55*, 1159–1172.

Ozawa, H., Hirose, K., Tateno, S., Sata, N., & Ohishi, Y. (2010). Phase transition boundary between B1 and B8 structures of FeO up to 210 GPa. *Physics of the Earth and Planetary Interiors*, *179*, 157–163.

Ozawa, H., Hirose, K., Yonemitsu, K., & Ohishi, Y. (2016). High–pressure melting experiments on Fe–Si alloys and implications for silicon as a light element in the core. *Earth and Planetary Science Letters*, *456*, 47–54.

Shahar, A., Ziegler, K., Young, E. D., Ricolleau, A., Schauble, E. A., & Fei, Y. (2009). Experimentally determined Si isotope fractionation between silicate and Fe metal and

379 implications for Earth's core formation. *Earth and Planetary Science Letters*, *288*, 228–
380 234.
381 Takahashi, S., Ohtani, E., Terasaki, H., Ito, Y., Shibazaki, Y., Ishii, M. et al. (2013). Phase
382 relations in the carbon-saturated C–Mg–Fe–Si–O system and C and Si solubility in
383 liquid Fe at high pressure and temperature: implications for planetary interiors. *Physics*
384 *and Chemistry of Minerals*, *40*, 647–657.
385 Umemoto, K., & Hirose, K. (2020). Chemical compositions of the outer core examined by
386 first principles calculations. *Earth and Planetary Science Letters*, *531*, 116009.
387 Vočadlo, L., Alfè, D., Gillan, M. J., & Price, G. D. (2003). The properties of iron under
388 core conditions from first principles calculations. *Physics of the Earth and Planetary*
389 *Interiors*, *140*, 101–125.
390 Yokoo, S., Hirose, K., Sinmyo, R., & Tagawa, S. (2019). Melting experiments on liquidus
391 phase relations in the Fe–S–O ternary system under core pressures. *Geophysical*
392 *Research Letters*, *46*, 5137–5145.

393 **Figure captions**

394

395 **Figure 1.** Temperature profile across a laser-heated spot (a) and images (b–d) of a sample
396 cross-section parallel to the compression and laser-heating axes from run #2 performed at
397 47 GPa. Temperature at the liquid-solid boundary is obtained (a), considering identical
398 temperature for both sides. Scanning ion microscope (SIM) image (b), and X-ray maps for
399 iron (green) + silicon (red) (c) and for carbon (d). Note that the contrast in the SIM image
400 reflects not only the mean atomic number but also crystallographic orientation. Scale bars
401 are 20 μm.

402

403 **Figure 2.** (a–c) Liquidus phase relations in the Fe-Si-C system at (a) ~50 GPa, (b) ~136
404 GPa, (c) ~200 GPa, and (d) their extrapolation to 330 GPa. Liquids coexisted with Fe
405 (reversed triangles), Fe-Si (triangles), Fe+Fe-Si (open diamond), and Fe+Fe_3C (closed
406 diamond). Fe_7C_3 appears as a liquidus phase above 200–250 GPa (Mashino et al., 2019).
407 Red, this study; blue, originally reported in Ozawa et al. (2016); black, Miozzi et al. (2020).
408 The Fe-C eutectic composition at respective pressure is given by a green bar considering its
409 uncertainty (Mashino et al., 2019). The cotectic lines are drawn considering the Fe-Si
410 binary eutectic composition (see Figure 3). Numbers indicate temperatures. The liquidus
411 field of Fe at ICB conditions is shown by an orange area in (d). (e, f) Si and C
412 concentrations in Fe-Si-C-1.7wt%S liquids in equilibrium with the inner core with possible
413 compositions proposed by Li et al. (2018). Calculations are based on D_C = 0.1 (e) and 0.2
414 (f). Red, black, and blue correspond to the inner core compositions respectively when
415 T_{360GPa} = 6500 K, 6000 K, and 5500 K. See text for details. Liquidus fields at 330 GPa are
416 illustrated by red lines.

417

418 **Figure 3.** Change in Si concentration in the Fe-Si binary eutectic liquids with increasing
419 pressure (red curve). The lower (triangles) and upper bounds (reversed triangles) are given
420 not only by Si concentration in liquid but also by the maximum Si content in solid Fe and
421 the minimum in solid Fe-Si, respectively, at each pressure (see text). The red curve is
422 constrained also by the position of Fe + Fe-Si cotectic line in the Fe-Si-C ternary liquidus
423 diagram (Fig. 2). The results of previous studies by Ozawa et al. (2016) (blue symbols, gray
424 curve) and Fischer et al. (2012, 2013) (green symbols) are similarly plotted. The

discrepancy between Ozawa et a. (2016) and this study is attributed to the fact that the presence of carbon was not considered in the former.

Figure 4. Partition coefficients for (a) C and (b) Si (D_C and D_{Si}) by weight between solid and liquid Fe, plotted as functions of Si and C concentrations in liquid, respectively, obtained at 34–199 GPa in this study. D_C in the Si-free system (a) and D_{Si} in the C-free system (b) are shown by open squares (Mashino et al., 2019) and an open circle (Kuwayama & Hirose, 2004), respectively. Numbers indicate pressure (GPa) and temperature (K) condition for each datum. A black broken line in (b) represents data at 1 bar for bcc Fe (Hino and Ito, 2010). The red line indicates the remarkable effect of C on D_{Si}, in particular for fcc and hcp Fe at high pressures.

Figure 1.

a

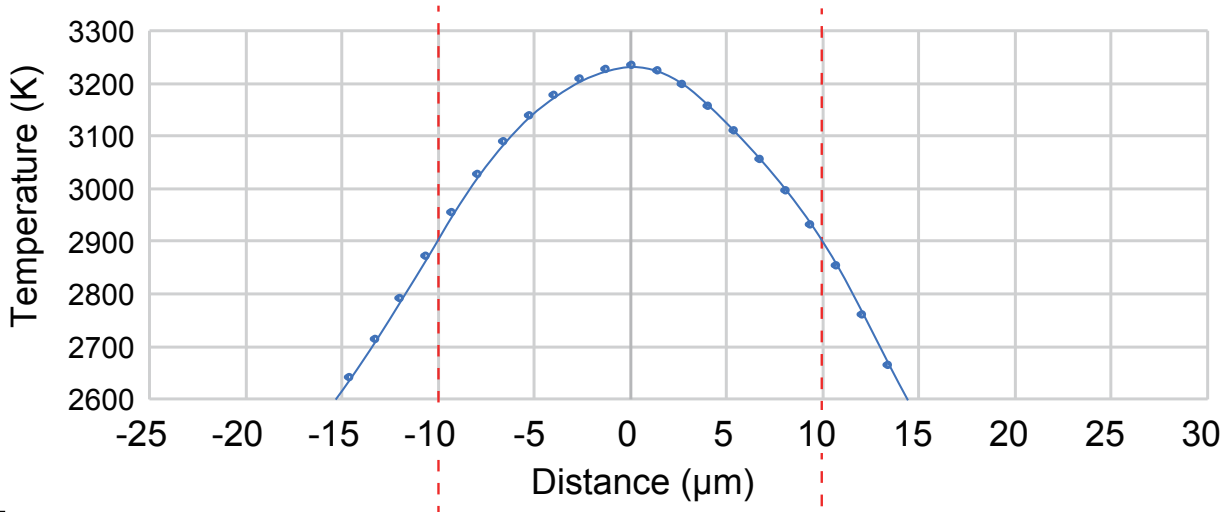
Temperature (K)
3300
3200
3100
3000
2900
2800
2700
2600
-25
-20
-15
-10
-5
0
5
10
15
20
25
30
Distance (μm)

b

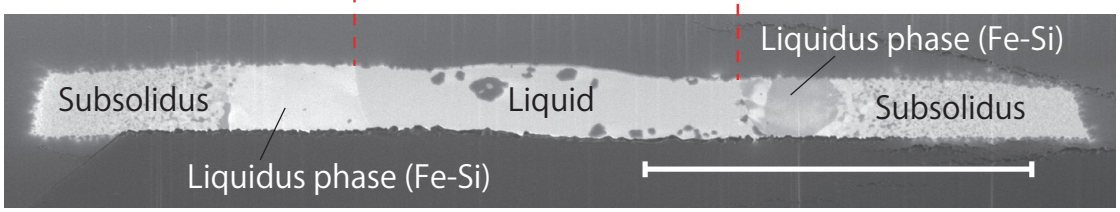
Liquidus phase (Fe-Si)
Subsolidus
Liquid
Subsolidus
Liquidus phase (Fe-Si)

c

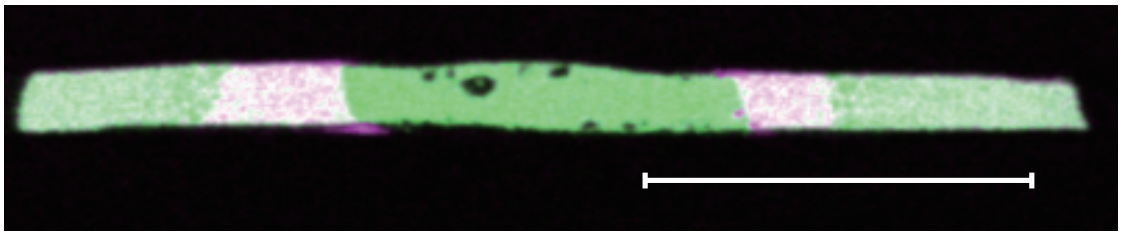

d

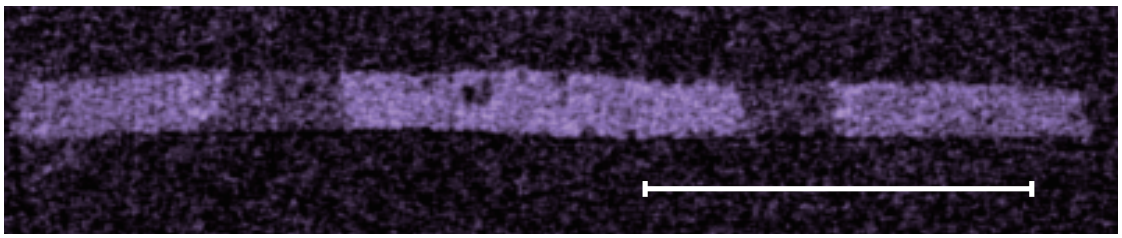

Figure 2.

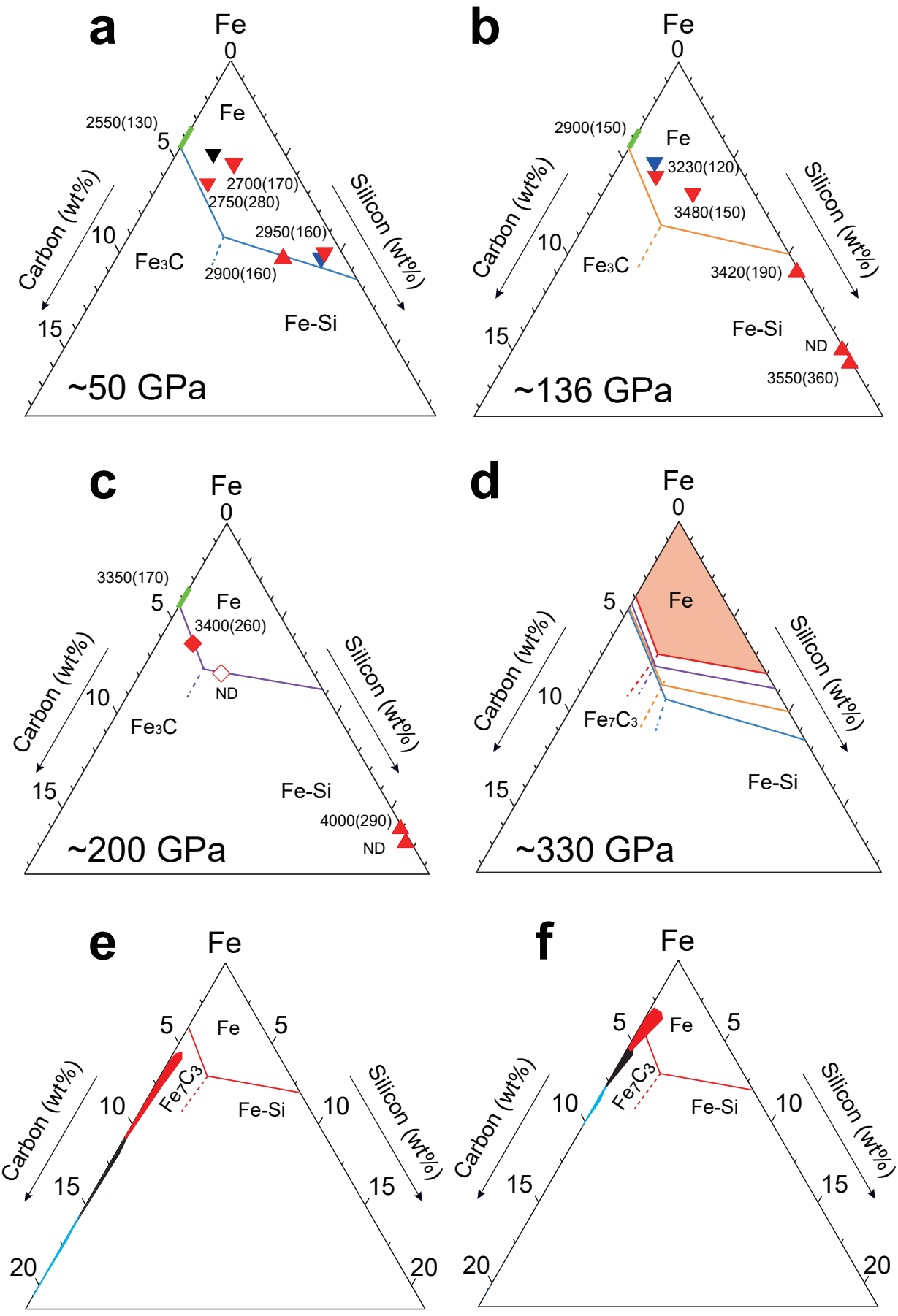
a
Fe
0
Fe
2550(130)
5
2700(170)
2750(280)
2950(160)
Carbon (wt%)
10
Fe3C
2900(160)
Silicon (wt%)
15
Fe-Si
~50 GPa
b
Fe
0
2900(150)
Fe
3230(120)
3480(150)
Carbon (wt%)
10
Fe3C
3420(190)
Silicon (wt%)
15
Fe-Si
ND
3550(360)
~136 GPa
c
Fe
0
3350(170)
5
Fe
3400(260)
ND
Carbon (wt%)
10
Fe3C
Silicon (wt%)
15
Fe-Si
4000(290)
ND
~200 GPa
d
Fe
0
5
Fe
Carbon (wt%)
10
Fe7C3
Silicon (wt%)
15
Fe-Si
~330 GPa
e
Fe
5
Fe
5
Carbon (wt%)
10
Fe7C3
Fe-Si
10
Silicon (wt%)
15
15
20
20
f
Fe
5
Fe
5
Carbon (wt%)
10
Fe7C3
Fe-Si
10
Silicon (wt%)
15
15
20
20

Figure 3.

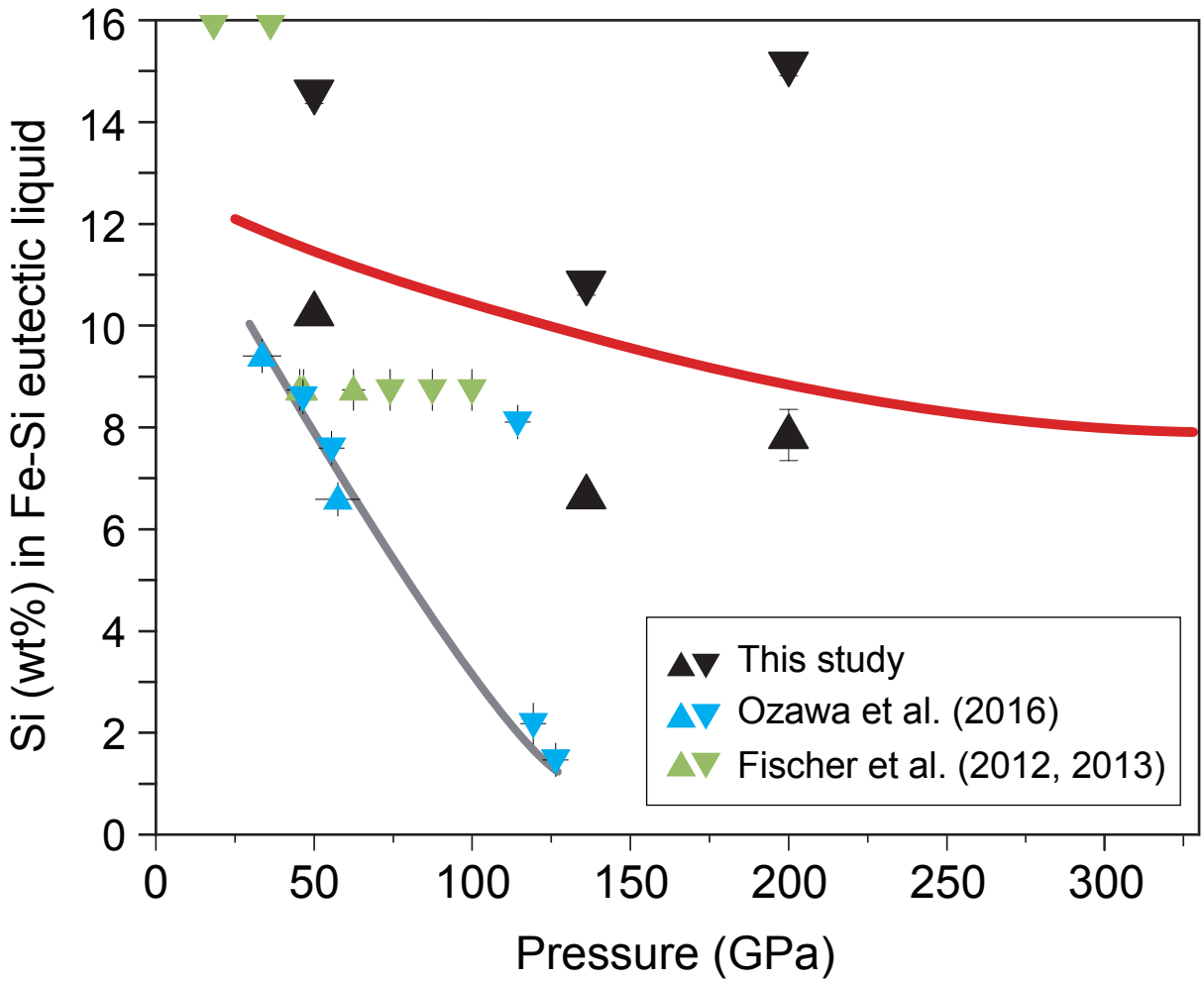
Si (wt%) in Fe-Si eutectic liquid
Pressure (GPa)
0
2
4
6
8
10
12
14
16
0
50
100
150
200
250
300
This study
Ozawa et al. (2016)
Fischer et al. (2012, 2013)

Figure 4.

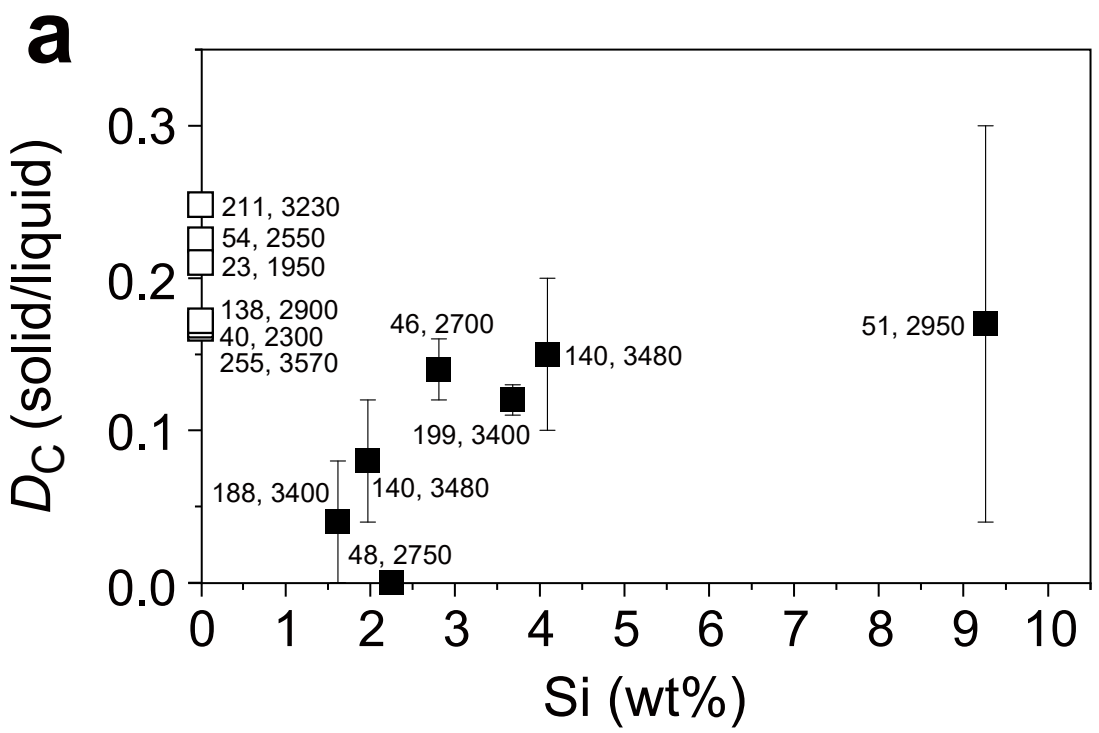
a
D_C (solid/liquid)
0.0
0.1
0.2
0.3
211, 3230
54, 2550
23, 1950
138, 2900
40, 2300
255, 3570
46, 2700
140, 3480
199, 3400
188, 3400
140, 3480
48, 2750
51, 2950
0
1
2
3
4
5
6
7
8
9
10
Si (wt%)

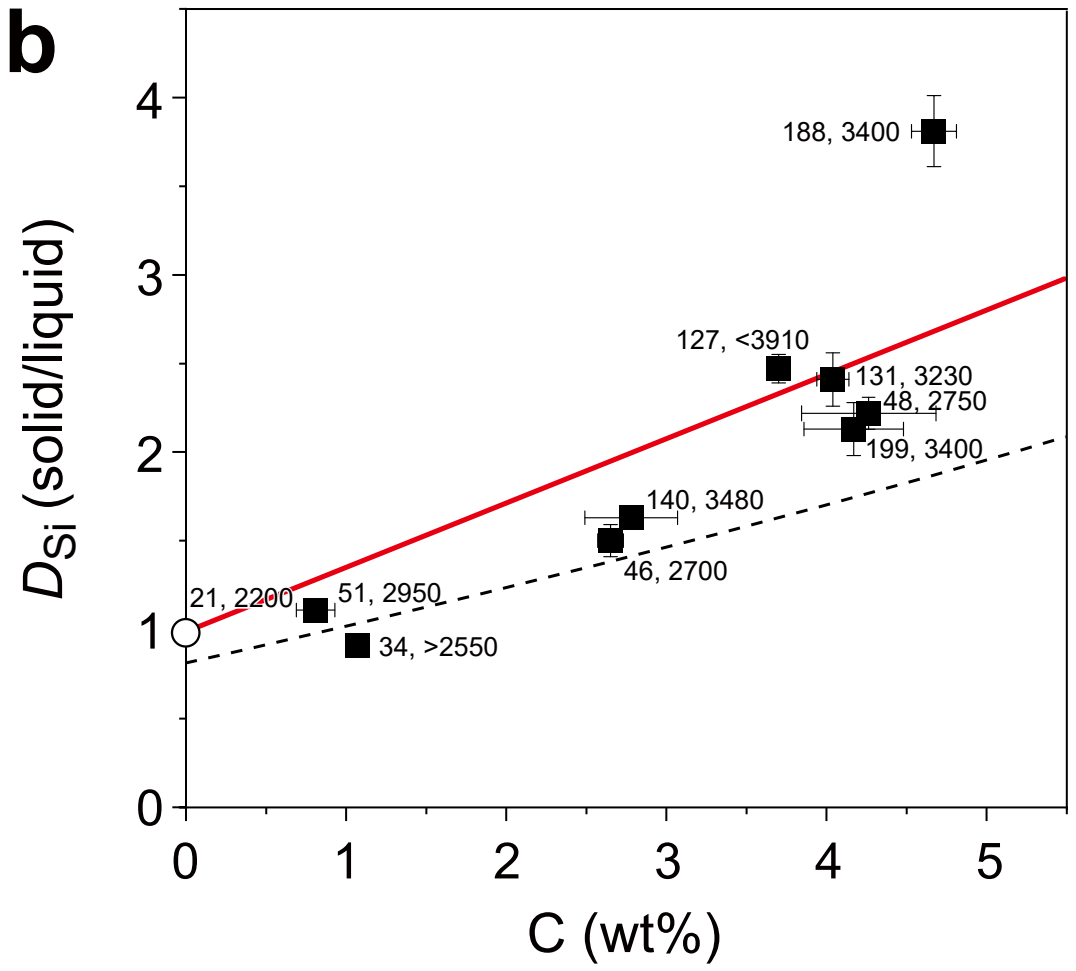
b
D_{Si} (solid/liquid)
0
1
2
3
4
188, 3400
127, <3910
131, 3230
48, 2750
199, 3400
140, 3480
46, 2700
21, 2200
51, 2950
34, >2550
0
1
2
3
4
5
C (wt%)